

SEPARATION ANGLE INFLUENCE IN THE NEAR WAKE OF 2-D BLUFF BODY

Tiago Barbosa de Araújo, araujotb@ita.br

Roberto da Mota Girardi, girardi@ita.br

Instituto Tecnológico de Aeronáutica, Praça Mal. do ar Eduardo Gomes, 50, Vila das Acácias - São José dos Campos - SP - Brazil

Abstract. *The two-dimensional flow features of bluff bodies have a strong relationship with the formation region (or near wake) parameters, such as its width, which are also related to the body shape. Because of the shape the flow direction on the separation point can vary, from parallel to perpendicular to the free stream. These changes on the flow direction can modify the width of the wake and consequentially other parameters, such as the base pressure coefficient, drag coefficient and the Strouhal number. In this paper we aim to show the influence of the flow separation angle in the near wake of wedges models. However the measurements in the region of base flow have specific features that make it harder, because of the recirculation zone formed at the body rear, which has very low velocities associated. Then, to make these measurements we use a laser Doppler anemometer. This equipment doesn't need calibration and can separate the velocities components. By using it the mean (u and v) and fluctuant (u_{RMS} and v_{RMS}) velocities fields were measured for the Reynolds number of 3.0×10^3 . Using these velocities fields is possible to determine some near wake parameters and their relation with another flow features.*

Keywords: *Bluff body, near wake, separation angle, LDA*

1. Introduction

Despite decades of studies the flow over bluff bodies still has some features that remain completely not understood. During this long period many authors have tried to correlate flow parameters among themselves, to establish some kind of similarity over a large range of different bodies shape wakes, such authors as Roshko (1954a) and Bearman (1965), who has used experimental approaches. In these experiments these authors, as others after them, observed that the near wake, or formation region, is a critical region where some interference leads to flow parameters modifications, such as drag reduction.

Roshko (1954b) also tried to obtain results theoretically, for the drag coefficient, using a modified hodograph method. He proposed a modification in Kirchhoff's free streamline theory to add wake characteristics. However, despite his efforts, the solution obtained was still dependent from the experiment for providing the base parameter (K), which is necessary in his solution. Girardi (1990) used the energy equation to obtain the drag coefficient, however its solution was also dependent from K . In both works the authors obtain the drag coefficient as a function of the ration between the wake width and the base body length.

After all, the most important here is the fact that the flow features, such as Strouhal number and base pressure coefficient, have a strong relationship with the near wake flow. Among others, the body shape is really important to setting the flow parameters, once it determines the detachment points, which in turn determines the wake width.

One of the most important and studied bluff bodies, the circular cylinder, is a great example of detachment points importance. To this body it is known that during the Reynolds number increasing the drag coefficient is incremented, but suddenly it decreases quickly, due to the separation point movement to the body rear part (Roshko, 1961). The body shape, and consequently the separation angle, variation can also interfere on the flow parameters as we can note just observing the drag coefficient reduction. For example, the flow over a transversal flat plate and a 45° apex angle wedge, for the same Reynolds number, give us the drag coefficients of 1.81 to 1.62 (Sousa, 1993), respectively.

The aim of this paper is present is show the changes in the near due to the separation angle variation. Thus, we are going to present the mean (u and v) and fluctuant (u_{RMS} and v_{RMS}) velocities fields. To measure these flow fields a laser Doppler anemometer (*LDA*) is used, because the flow characteristics at the formation region, very low velocities and reverse flow. The *LDA* is more suitable than the hot wire anemometer, because it does not need calibration, can distinguish the velocity components and is non-intrusive (Jensen, 2004).

2. Experimental Apparatus

The measurements were performed in an open circuit wind tunnel, where the fan is placed after the test section, manufactured by *TSI* (model 8390), as we can see in fig. 1. Its test section is square and characterized by the dimension of 101.6 millimeters. The flow velocity ranges from 1.0 *m/s* to 32.0 *m/s* and 1.2% turbulence level at maximum speed with flow seeding presence.

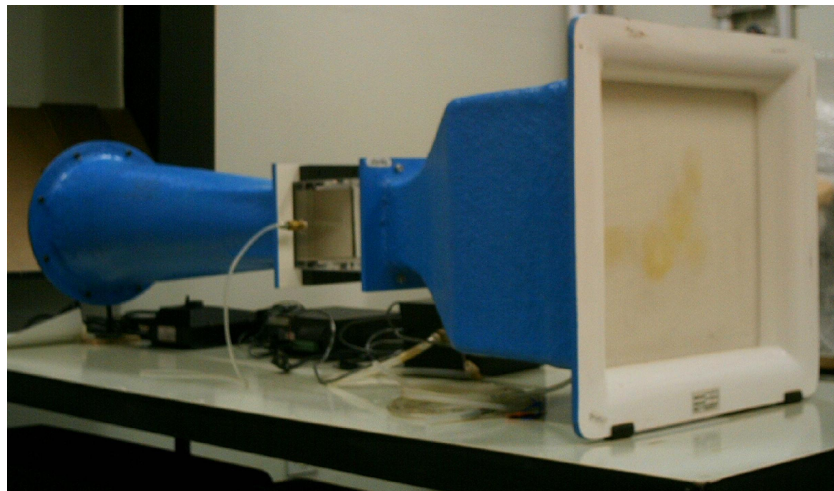


Figure 1. Wind tunnel model 8390 with square test section characterized by the dimension of 101.6 mm.

The models used in this work were wedges with three different separation angles, 15°, 30° e 45° (see fig. 2), with the same blockage ratio, 9.8%. All models aspect ratio are equal to 10.2, which the end effects can't be neglected, but only at the mean span, where the measurements are taken (Mittal, 2001).

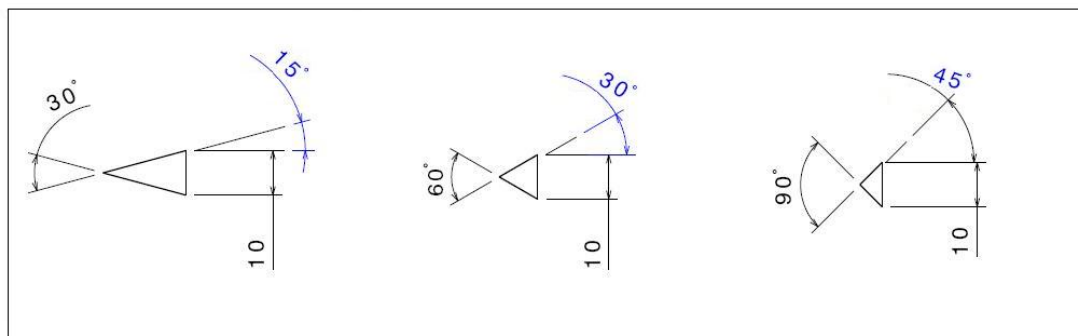


Figure 2. Lateral view of the three different wedges.

The models are placed in the test section in such a way that they stay perpendicular to the plane XOY , as shown in the Fig. 3.

To perform the flow measurements was used a LDA system equipped with an Argon-Krypton laser. This LDA is able to make three-dimensional measurements, however as the mean span flow can be said two-dimensional, we have opted by using the 2D configuration. In the figure 4, is presented the system picture with its parts labeled. The LDA probe was mounted on a bench, which was placed together on two-dimensional traverse with 0.1 mm precision.

The flow seeding utilized in this work were olive oil which was atomized in particle generator made by TSI (model 9307). This generator was calibrated to produce droplets with mean diameter of 1.0 μm which are suitable for low Mach number regimes and for turbulent flow with 10 KHz maximum frequency (Melling, 1997). The dynamic pressure was controlled by a WIKA (Tronic Line) micromanometer which ranges from 0.0 mbar to 1.0 mbar (100,0 Pa). This was calibrated from 0.0 m/s to 12.0 m/s. For more detailed description of this experimental apparatus can be seen in Araújo and Girardi (2009).

3. Experimental Procedure

In the figure 3, beyond the coordinate system we can also see four distances, a , b , c and d , that is used to model alignment. First using a set-square the model is placed perpendicular to the test section lower surface. After the distances from both model ends to the test section upper surface are measured with digital caliper, until the distances a and b are set equal.

In the next step, the distances from the model ends to the test section end are performed until the distances c and d are set equal. With these four distances adjusted the set-square is place against the base body surface again, to ensure its perpendicularity, and the distances are checked. If some of these is not correct, the previous steps are repeated until the distances and the perpendicularity are set right and the alignment be done.

After the models alignment we have to ensure that the measurement volume is placed at model middle-span and the

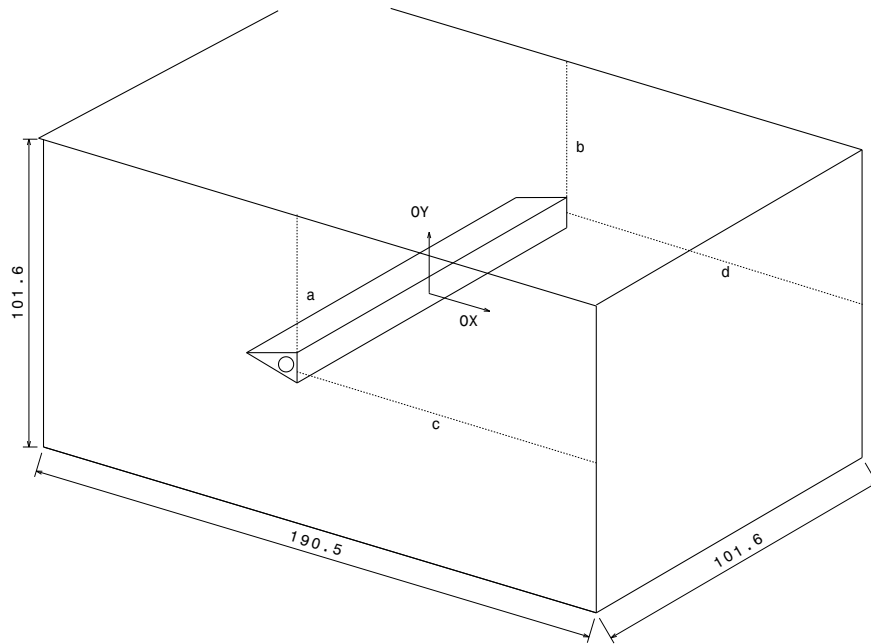


Figure 3. Test section view with a model placed at its position, showing the coordinate system adopted.

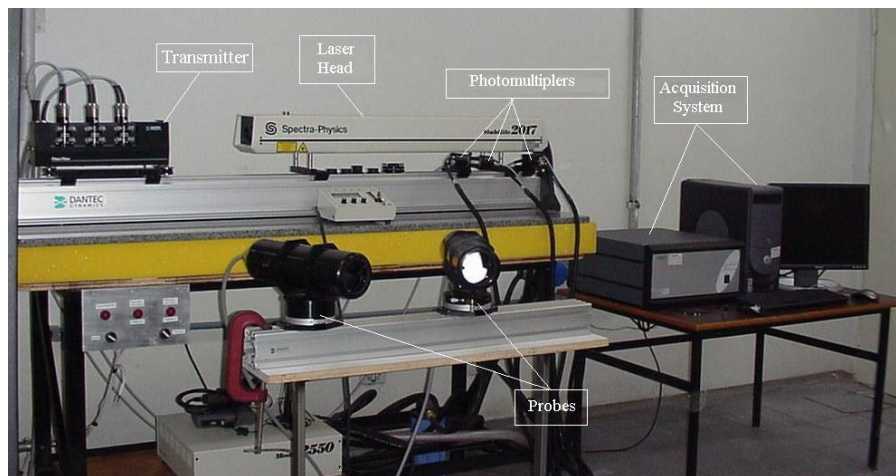


Figure 4. General view of the LDA setup.

wind tunnel is aligned to the *LDA* coordinate system (see Araújo and Girardi, 2009). Then, with the measurement time defined (see Araújo and Girardi, 2008) to the flow inside and outside the wake, 64 seconds and 32 seconds respectively, the velocity profiles are taken in *y*-direction.

The coordinate system is set from the definition of its three directions as follow. The *y*-direction as the direction parallel to the base model pointing to the wind tunnel upper surface, the *x*-direction is the freestream flow direction and the *z* direction is the span direction. The profiles measurements are taken in the plane *XOY* keeping the *z*-direction constant.

With the origin set at the middle-span and half base length model the profile is started at $0.2d$ and goes until $1.2d$ by increments of $0.1d$, except to the separation point region where the mesh is refined and the increments are of $0.05d$. Finishing the profile measurement, the traverse system is moved at the *x*-direction by the increment of $0.1d$ and a new profile is taken. This increments is kept constant from the origin to $2.0d$, after it becomes $0.2d$ until $3.0d$.

The procedure describe in the previous paragraph is repeated until all the measurements are taken, completing the entire mesh defined.

4. Results

In this section we are going to present the flow fields obtained for the three different separation angle wedges, keeping the Reynolds number and the blockage ratio constant, for zero angle of attack. We start with the non-dimensional vorticity field, defined by the eq. 1 and presented in the figure 5. In this figure the letters N and S represent the vortex core and the

saddle point approximated position, respectively.

$$\omega_z = \frac{1}{2} \left(\frac{\partial v}{\partial x} - \frac{\partial u}{\partial y} \right) \quad (1)$$

From this figure we can see that the vorticity is well concentrated near the separation point, where the shear layer leaves the body, keeping itself like that, until the mean vortex core region, spreading out after. We can also observe from it, that increasing the separation angle makes the negative vorticity maximum becomes more negative. This decrement can be related to model shape, which deflects more the flow with the separation angle increases, causing larger velocities variation on x and y directions. The vorticity increase can also be noted on the vortex strength, defined by equation 2, behavior which increases with the separation angle increment (see table 1).

$$\frac{\Gamma}{U_\infty d} = \frac{K^2}{2St} \quad (2)$$

Where St is the Strouhal number and K is the base pressure parameter (Fage and Johansen, 1927), given by:

$$C_{pb} = 1 - K^2 \quad (3)$$

The flow deflection cited before creates an effective body with slightly larger base length, as can be observed from the mean vortex core displacement in the y -direction. This deflection let larger area to be fulfilled by the flow in the body base, leading to a mean vortex size increment, as we can observe by the Strouhal number decrement, with the separation angle increasing, shown in the Tab. 1. The Strouhal number (St) decrement indicates a larger vortex formation time. In the table 1 are presented the mean flow parameters variation with the separation angle increment.

Table 1. Parameter variation with the separation angle increment.

ϕ	$\frac{X_N}{d}$	$\frac{Y_N}{d}$	$\frac{X_{ur}}{d}$	$\frac{Y_{ur}}{d}$	$\frac{X_{vr}}{d}$	$\frac{l_S}{d}$	K	C_{Pb}	St	$\frac{\Gamma}{U_\infty d}$
15°	0,73	0,26	1,0	0,3	1,5	1,3	1,313	-0,72	0,233	3,70
30°	0,86	0,33	1,1	0,4	1,7	1,6	1,398	-0,95	0,194	5,04
45°	0,83	0,35	0,9	0,4	1,9	1,5	1,394	-0,94	0,184	5,28

We can also see that the mean vortex core x -position (X_N/d) increases when the separation angle grows from 15° to 30° and then stays approximately constant for the second increment. This behavior can also be noted on base pressure coefficient (C_{pb}) modulus, showing a good correlation between C_{pb} and X_N/d .

Simmons (1977) has published a paper where he studies the variation on the formation region length, by the maximum longitudinal fluctuation velocity criteria (Bearman, 1965), with the separation angle. In this paper the author presents results for the 15° and 30° wedges at the Reynolds number of 1.5×10^4 , but the first one posses a rounded leading edge. In these conditions he obtained Strouhal numbers of 0.24 e 0.20 for the wedges of 15° and 30°, respectively. Besides the Reynolds number, these results are in good agreement with the presented in the table 1. For the 45° wedge the St obtained by Roshko (1954a) is 0.179, but his measurement were taken at Re equal to 3.9×10^3 .

From the figure 6 to 8, are present the mean and fluctuant velocity fields, for the three different bodies. The letters A, B and C indicates the maximum longitudinal fluctuant velocity position (X_{ur}/d) and D, E and F represents the maximum transversal fluctuant velocity position (X_{vr}/d). We have to mention that these maximums are not well pronounced peak and the points around it are inside the uncertainty (presented with 95% of probability).

In the figure 6 are presented the longitudinal (u/U_∞) mean velocity fields. In these figures we can see the maximum velocity increasing with the separation angle increment. This increment in the mean velocity is reflected in the base pressure coefficient behavior, because the maximum is found at the separation point.

We can also observe from the streamlines on figure 6 that the mean recirculation bubble grows up from 15° to 30° and kept almost constant for the next increment in the separation angle. However, for the variation from 30° to 45° we can observe a topological change in the mean vortex core position, which moves up and forward the body base. The separation angle increment forces the flow deflection, creating a larger effective base body, this elevates the mean core position (y -direction). In the other hand, the increment in the mean vortex, observed by the Strouhal number decrement, increases the volume occupied by itself, leading to x -position increment.

In the figures 7 and 8 are presented the longitudinal (u_{RMS}/U_∞) and transversal (v_{RMS}/U_∞) fluctuant velocity fields. We can note from these figures that there is an increment on maximum fluctuations for both velocity fields. The growing mean vortex strength with the separation angle variation causes larger induced velocities leading to greater RMS values.

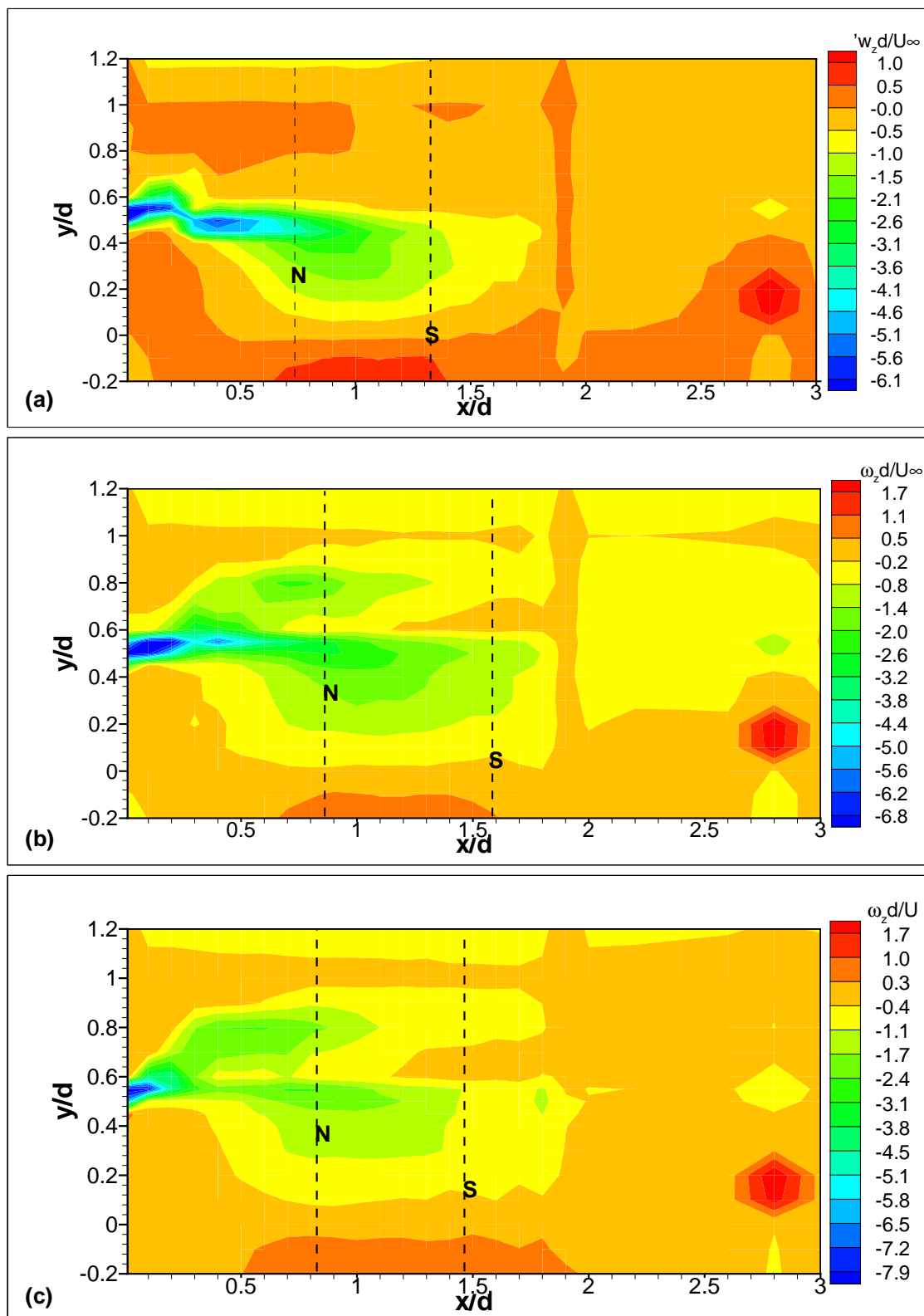


Figure 5. Non-dimensional vorticity field for the separation angles of (a) 15° , (b) 30° and (c) 45° with non-dimensional uncertainty of 32%, 38% and 29%, respectively. All uncertainties with 95% of probability

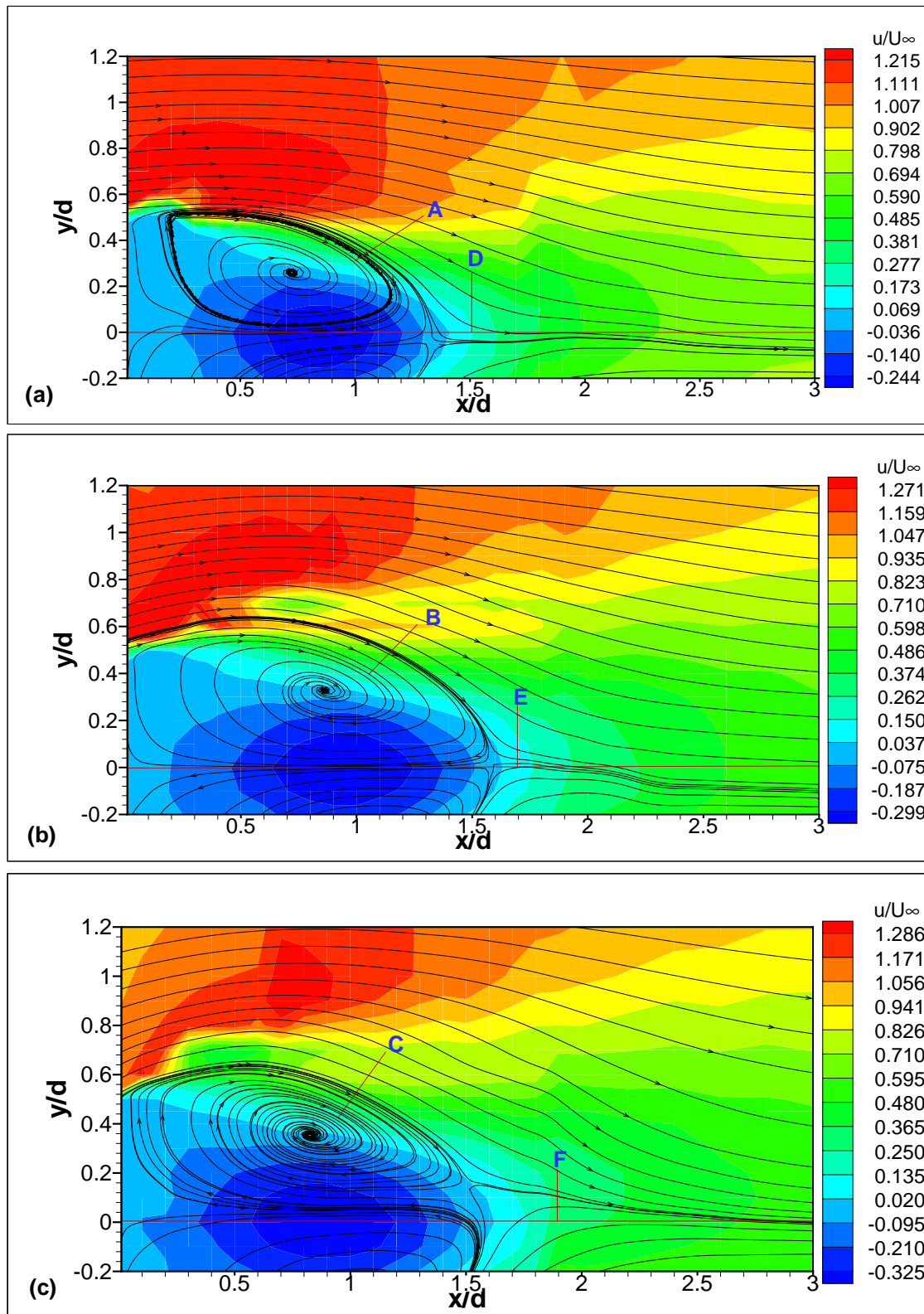


Figure 6. Longitudinal mean velocity field with stream lines for the separation angles of (a) 15° (non-dimensional uncertainty of ± 0.002), (b) 30° (non-dimensional uncertainty of ± 0.004) and (c) 45° (non-dimensional uncertainty of ± 0.003).

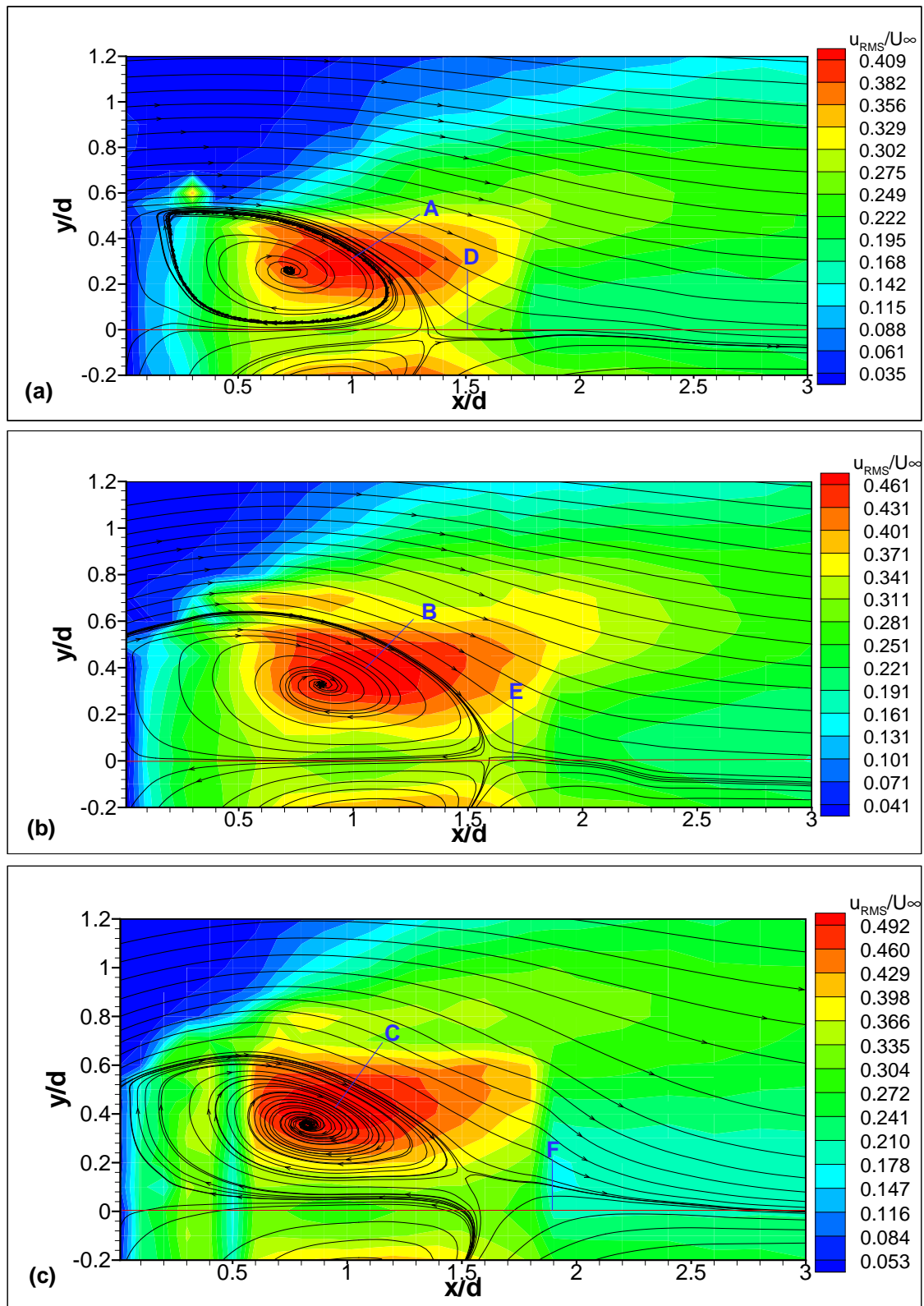


Figure 7. Longitudinal fluctuant velocity field with stream lines for the separation angles of (a)15° (non-dimensional uncertainty of ± 0.001), (b) 30°(non-dimensional uncertainty of ± 0.003) and (c) 45°(non-dimensional uncertainty of ± 0.002).

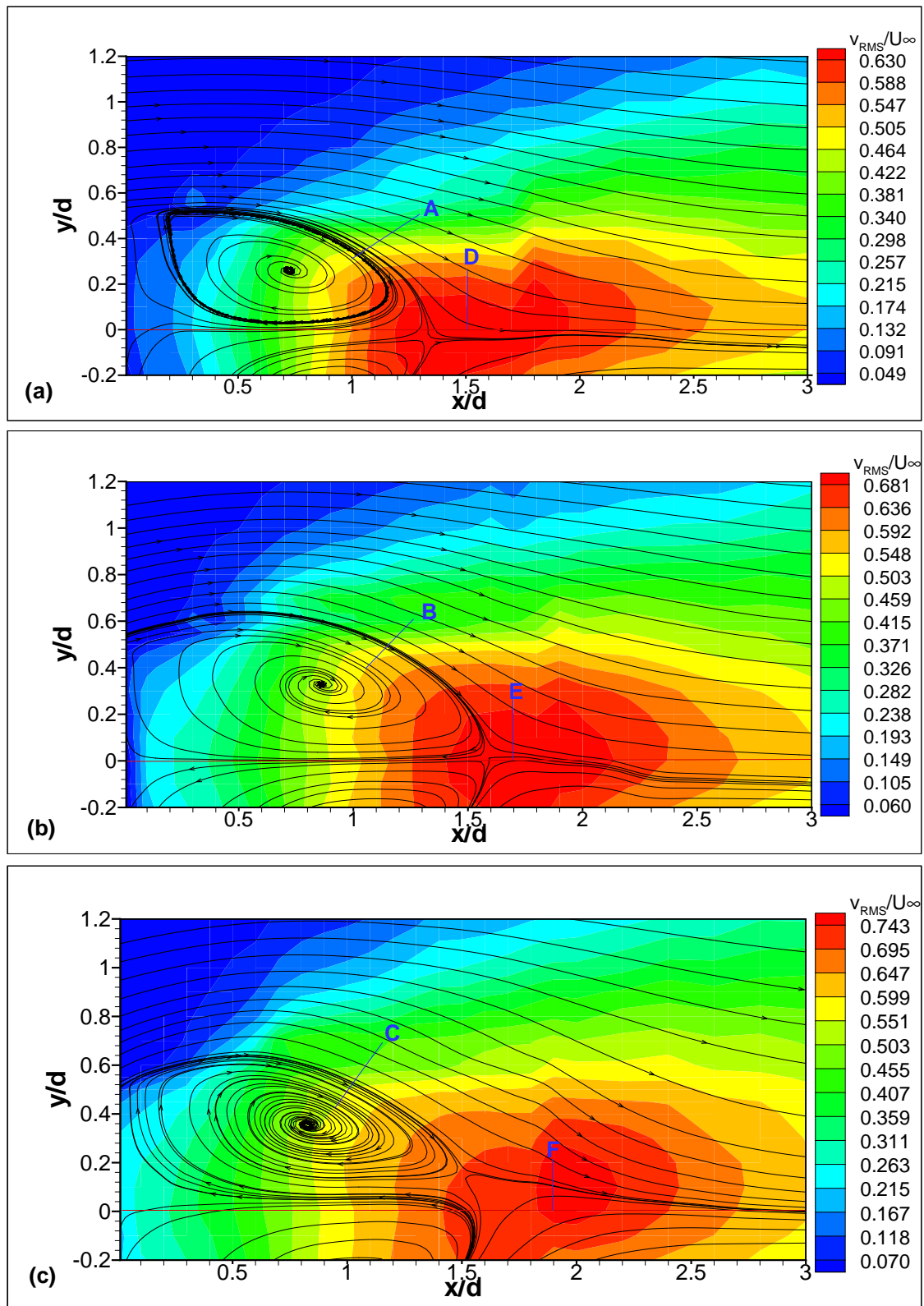


Figure 8. Transversal fluctuant velocity field with stream lines for the separation angles of (a)15° (non-dimensional uncertainty of ± 0.003), (b) 30°(non-dimensional uncertainty of ± 0.005) and (c) 45°(non-dimensional uncertainty of ± 0.004).

From the figure 7 we can observe that the maximum u_{RMS} position (X_{ur}/d) changes just a little bit with the separation angle increment. The displacement observed due to each angle increment is within our uncertainty, as explained before, making impossible any concrete conclusion about the formation length variation.

Simmons (1977) also presented results for the formation length, based in the same criteria of maximum u_{RMS} , for the wedges of 15° and 30° , which were of 1.0 and 1.15, respectively, been close to our values. Although, we cannot ensure the results presented in this paper, due to uncertainty. This, is due to the absence of well defined peak in the results.

From the figure 8 we observe that the maximum v_{RMS} position, X_{vr}/d only grows with the separation angle increment, as the mean vortex strength. Despite of uncertainty presented, we can ensure the v_{RMS} tendency, once the displacements for each angle increment is larger than 0.1.

5. Final Remarks

As we could observe in the results presented in this paper, the use of laser Doppler anemometry improves the measurements giving us not only the mean velocity fields, but also the fluctuant ones, which can both be used for computational methods validation. The vorticity field, obtained from experimental data in this paper, is very sensitive to the displacement measurements, what makes its uncertainty large. Then, to make these uncertainties smaller, is necessary the experimental apparatus improvement.

The values shown in the table 1 present good agreement among themselves, mainly the values for X_N/d , X_{ur}/d and l_S/d , which have the same behavior. The measurements shown presented a good agreement with the results of Simmons (1977) for 15° and 30° separation angle wedges and Roshko (1961) for 45° wedge. The separation angle variation causes a mean vortex growing and topological alterations in the near wake.

6. Acknowledgements

To Coordenação de Aperfeiçoamento de Pessoal de Nível Superior (CAPES) and to Fundação Casimiro Montenegro Filho, for supporting part of the resources used in this research. To all the staff of the Prof. K.L. Feng Aeronautical Engineering Laboratory. To FAPESP and EMBRAER for the financial support used to acquire the LDA equipment.

7. References

- Araújo, T.B. and Girardi, R.M., 2008, "Laser Doppler anemometry application for wedges near wake study", Proceedings of 12th Brazilian Congress of Thermal Engineering and Sciences, vol. 1, Belo Horizonte, Brazil.
- Araújo, T.B. and Girardi, R.M., 2009, "Blockage Ratio Influence in 2-D Bluff Body Near Wake at Low Reynolds Number", Proceedings of 20th International Congress of Mechanical Engineering, Gramado, Brazil.
- Bearman, P.W., 1965, "Investigation of flow behind a two-dimensional model with a blunt trailing edge and fitted with splitter plates", Journal of Fluid Mechanics, Vol.21, pp. 241-255.
- Fage, A. and Johansen, F.C., 1927, "On the flow of air behind an inclined flat plate of infinite span", Proc. Roy. Soc., vol. 116, pp.170-197.
- Girardi, R.M., "Modelo Aerodinâmico do Escoamento Plano sobre Corpos Rombudos", PhD thesis - Instituto Tecnológico de Aeronáutica, 1990.
- Jensen, K. D., 2004, "Flow measurements", J. of the Brazilian Soc. Mechanics Sciences and Engineering, Vol.26, pp. 400-419.
- Melling, A., 1997, "Tracer particles and seeding for particle image velocimetry", Meas. Sci. Technol. Vol.8, pp.1406-1416
- Mittal, S., 2001, "Computation of three-dimensional flow past circular cylinder of low aspect ratio", Physics of Fluids, Vol.13, pp. 177-191.
- Roshko, A., 1954a, "On the Drag and Shedding Frequency of Two-dimensional Bluff Bodies", NACA Technical Note 3169.
- Roshko, A., 1954b, "A New Hodograph for Free-streamline theory", NACA Technical Note 3168.
- Roshko, A., 1961, "Experiments on Flow Past a Circular Cylinder at Very High Reynolds Number", Journal of Fluid Mechanics, Vol. 10, pp. 345-356.
- Simmons, J.E.L., 1977, "Similiarties Between Two-Dimensional and Axisymmetric Vortex Wakes", Aeronautical Quarterly, Vol. 28, pp. 15-20.
- Sousa, F.L., 1993, "Influência da razão de bloqueio no escoamento plano sobre corpos rombudos", Msc Thesis - Instituto Tecnológico de Aeronáutica.

8. Responsibility notice

The author(s) is (are) the only responsible for the printed material included in this paper